A Physiologically-Based Pharmacokinetic Model for Cannabidiol in Healthy Adults, Hepatically-Impaired Adults, and Children[S]

Sumit Bansal, [iD]Mayur K. Ladumor, [iD]Mary F. Paine, and [iD]Jashvant D. Unadkat

Department of Pharmaceutics, University of Washington, Seattle, Washington (S.B., M.K.L., J.D.U.); Department of Pharmaceutical Sciences, College of Pharmacy and Pharmaceutical Sciences, Washington State University, Spokane, Washington (M.F.P.); and Center of Excellence for Natural Product Drug Interaction Research (M.F.P., J.D.U.)

ABSTRACT

Cannabidiol (CBD) is available as a prescription oral drug that is indicated for the treatment of some types of epilepsy in children and adults. CBD is also available over-the-counter and is used to self-treat a variety of other ailments, including pain, anxiety, and insomnia. Accordingly, CBD may be consumed with other medications, resulting in possible CBD-drug interactions. Such interactions can be predicted in healthy and hepatically-impaired (HI) adults and in children through physiologically based pharmacokinetic (PBPK) modeling and simulation. These PBPK models must be populated with CBD-specific parameters, including the enzymes that metabolize CBD in adults. In vitro reaction phenotyping experiments showed that UDP-glucuronosyltransferases (UGTs, 80%), particularly UGT2B7 (64%), were the major contributors to CBD metabolism in adult human liver microsomes. Among the cytochrome P450s (CYPs) tested, CYP2C19 (5.7%) and CYP3A (6.5%) were the major CYPs responsible for CBD metabolism.

Using these and other physicochemical parameters, a CBD PBPK model was developed and validated for healthy adults. This model was then extended to predict CBD systemic exposure in HI adults and children. Our PBPK model successfully predicted CBD systemic exposure in both populations within 0.5- to 2-fold of the observed values. In conclusion, we developed and validated a PBPK model to predict CBD systemic exposure in healthy and HI adults and children. This model can be used to predict CBD-drug or CBD-drug-disease interactions in these populations.

SIGNIFICANCE STATEMENT

Our PBPK model successfully predicted CBD systemic exposure in healthy and hepatically-impaired adults, as well as children with epilepsy. This model could be used in the future to predict CBD-drug or CBD-drug-disease interactions in these special populations.

Introduction

Cannabidiol (CBD), a nonintoxicating phytocannabinoid, is approved in the United States (Epidiolex) and Europe (Epidyolex) as an oral solution for the treatment of some types of epilepsy, including Lennox-Gastaut syndrome, Dravet syndrome, or tuberous sclerosis complex (Devinsky et al., 2016). CBD is also available over-the-counter and is widely used by consumers to self-treat a variety of other ailments, including pain, anxiety, and insomnia.

The widespread use of CBD raises concern for potential clinically significant CBD-drug interactions, especially because CBD (750 mg orally twice daily) can be hepatotoxic, as evidenced by elevated serum alanine aminotransferase (Watkins et al., 2021). This alanine aminotransferase elevation is dose-dependent (10–20 mg/kg/d; Epidiolex

Package Insert) and is more pronounced in adult and pediatric patients who also take valproic acid, another hepatotoxin (Devinsky et al., 2018a; Meseguer et al., 2021). The United States Food and Drug Administration recommends monitoring serum alanine aminotransferase and bilirubin before initiating Epidiolex in patients taking valproic acid (Epidiolex Package Insert). In addition, compared with healthy adults, CBD systemic exposure (AUC and maximum systemic plasma clearance; C_{max}) is increased 1.5- to 4-fold in patients with mild, moderate, or severe hepatic impairment (Taylor et al., 2019). Thus, the widespread use of CBD raises concern for potential clinically significant CBD-drug and/or CBD-disease interactions.

CBD-drug interactions in healthy and hepatically-impaired (HI) adults and children could be predicted using physiologically based pharmacokinetic (PBPK) modeling and simulation. Once a CBD PBPK model has been developed and validated for these populations, the model can be used to predict CBD systemic exposure in other populations not studied, including younger children, the elderly, and pregnant people, and to predict CBD-drug interactions in healthy and HI adults and in children.

CBD is highly lipophilic (log P = 6.33) (ChEMBL database), has low aqueous solubility (0.0627 μg/ml), and has a poor oral bioavailability (8%), which is improved approximately 4-fold in the presence of a high-fat meal (Taylor et al., 2018, 2019; Koch et al., 2020; Perkins

ABBREVIATIONS: AUC, area under the plasma concentration versus time curve; CBD, cannabidiol; CI, confidence interval; CL_H, hepatic plasma clearance; CL_{int}, intrinsic clearance; CL_{IV}, intravenous plasma clearance; C_{max}, maximum systemic plasma concentration; CYP, cytochrome P450; F_a, fraction absorbed; f_m, fraction metabolized; $f_{u,p}$, unbound fraction in the plasma; HLM, human liver microsome; HI, hepatically-impaired; k_a, absorption rate constant; k_{dep}, depletion rate; k_{inact}, maximum inactivation rate constant; $K_{I,u}$, binding-corrected half-maximal inactivation constant; PBPK, physiologically based pharmacokinetic; 2-PPP, 2-phenyl-2-(1-piperidinyl)propane; UDPGA, UDP glucuronic acid; UGT, UDP-glucuronosyltransferase; V_{ss}, volume of distribution at steady state.

et al., 2020). CBD plasma AUC and C_{max} are dose-proportional when administered with a high-fat diet (Perkins et al., 2020) but are less than dose-proportional when administered under fasting conditions, which is likely due to the low aqueous solubility (Taylor et al., 2018). As in adults, CBD PK are dose-proportional in children (ages 4–10 years) when administered with food (Devinsky et al., 2018b). CBD is largely excreted in the feces, with minimal elimination in the urine (Epidiolex Package Insert). CBD is metabolized in the liver by cytochrome P450s (CYPs), including CYP1A, CYP2C9, CYP2C19, CYP2D6, and CYP3A (Jiang et al., 2011), and uridine 5′-diphospho-glucuronosyltransferases (UGTs), including UGT1A9 and UGT2B7 (Mazur et al., 2009). Of these CYPs, the fraction of CBD metabolized (f_m) by CYP2C9 (0.15), CYP2C19 (0.3), and CYP3A (0.54) has been quantified (Beers et al., 2021), but the overall contribution of CYPs and UGTs to the metabolism of CBD has not been quantified. Such data are necessary to build a PBPK model for CBD. CBD does not appear to be a substrate for transporters, including organic anion transporting polypeptide 1A2 and 2B1, P-glycoprotein, breast cancer resistance protein, and bile salt export pump (Epidiolex Package Insert).

The objective of the present study was to develop and validate a PBPK model for CBD in healthy and HI adults and in children using in vitro experimental (generated in-house) and published in vivo CBD PK data (available for children only for ages 4–10 years). Specifically, our aims were to a) determine the intrinsic clearance (CL_{int}) and fraction metabolized (f_m) of CBD by CYPs and UGTs using pooled human liver microsomes (HLMs); b) develop and validate a CBD PBPK model for healthy adults after oral CBD administration (fasted and fed conditions); and c) extend this validation to the HI adult and pediatric (4–10 years) populations.

Materials and Methods

Biologic Materials, Chemicals, and Reagents. Pooled HLMs prepared from 200 donors (mixed sexes) were obtained from SEKISUI Xenotech, LLC (Kansas City, KS). CBD was purchased from Cayman Chemical (Ann Arbor, MI). Methanolic solutions of deuterated CBD were purchased from Cerilliant (Round Rock, TX). Furafylline, UDP glucuronic acid (UDPGA), alamethicin, sulfaphenazole, digoxin, quinidine, and reduced β-nicotinamide adenine dinucleotide phosphate (NADPH) were purchased from Sigma-Aldrich (St. Louis, MO). Montelukast, benzylnirvanol, azamulin, 2-phenyl-2-(1-piperidinyl)propane (2-PPP), and β-phenyllongifolol were purchased from Toronto Research Chemicals (Toronto, ON, Canada). Bovine serum albumin (BSA), acetonitrile, and formic acid were purchased from Fisher Scientific (Hampton, NH). Ultralow-binding microcentrifuge tubes were purchased from Genesee Scientific (EI Cajon, CA).

CBD Depletion by CYPs and UGTs in HLMs. CBD (50 or 1000 nM) was incubated with pooled HLMs (0.3 mg/ml), with or without NADPH (1 mM), or HLMs (0.05 mg/ml), with or without UDPGA (2.5 mM), in 200 μl of potassium phosphate buffer (100 mM; pH 7.4) and bovine serum albumin (0.2%). Parallel incubations were conducted in the presence of a selective enzyme inhibitor or inactivator (Bichlmaier et al., 2007; Lapham et al., 2012, 2020): 10 μM of furafylline (CYP1A2), 3 μM of 2-phenyl-2-(1-piperidinyl)propane (2-PPP; CYP2B6), 0.7 μM of montelukast (CYP2C8), 10 μM of sulfaphenazole (CYP2C9), 3 μM of benzylnirvanol (CYP2C19), 1 μM of quinidine (CYP2D6), 3 μM of azamulin (CYP3A), 10 μM of digoxin (UGT1A9), or 3 μM of β-phenyllongifolol (UGT2B7). At the concentration used, each inhibitor has been shown to completely and selectively inhibit the respective CYP or UGT enzyme activity (Bichlmaier et al., 2007; Khojasteh et al., 2011; Lapham et al., 2012). Stock solutions of CBD and enzyme inhibitors or inactivators were prepared in DMSO (100%), of which the final concentration was always <1% v/v. Incubation mixtures (200 μl) containing CYP reversible inhibitors were pre-warmed for 5 minutes at 37°C in a heating block with constant stirring (300 rpm) prior to initiating the reaction with NADPH. Incubation mixtures containing CYP inactivators (furafylline or azamulin) were preincubated with NADPH for 20 minutes at 37°C to achieve complete inactivation of the respective CYP prior to the addition of CBD. Incubation mixtures containing UGT

inhibitors (all reversible) were pretreated with alamethicin (25 $\mu g/ml$) on ice for 15 minutes to allow pore formation. The mixtures were then prewarmed for 5 minutes at 37°C prior to initiating the reaction with UDPGA. At 0, 10, 20, or 30 minutes, the reaction was terminated by adding 30 μl of incubation mixture to 120 μl of acetonitrile containing the internal standard (deuterated CBD). Samples were vortexed then centrifuged at 18,000 g for 10 minutes to precipitate proteins. CBD was quantified in the supernatants using liquid chromatography-tandem mass spectrometry methods as described previously (Bansal et al., 2022). Two independent experiments were conducted, each in duplicate.

Data Analyses. The depletion rate constant (k_{dep}) was estimated by fitting a log-linear model to the percent of CBD remaining in the incubation in the absence or presence of CYP or UGT selective inhibitor (GraphPad Prism 6.01, San Diego, CA). The CBD intrinsic clearances by CYP ($CL_{int,CYPs}$) and UGT ($CL_{int,UGTs}$) were estimated using eqs. 1 and 2, respectively, where $k_{dep,NADPH}$ represents the rate of CBD depletion by CYPs in the presence of NADPH, $k_{dep,UDPGA}$ represents the rate of CBD depletion by UGTs in the presence of UDPGA, and [HLM] is the microsomal protein concentration.

$$CL_{int,CYPs} = \frac{k_{dep,NADPH}}{[HLM]} \quad (1)$$

$$CL_{int,UGTs} = \frac{k_{dep,UDPGA}}{[HLM]} \quad (2)$$

The fraction of CBD metabolized by CYPs and UGTs was calculated using eqs. 3 and 4, respectively:

$$f_{m,CYPs} = \frac{CL_{int,CYPs}}{CL_{int,CYPs} + CL_{int,UGTs}} \quad (3)$$

$$f_{m,UGTs} = \frac{CL_{int,UGTs}}{CL_{int,CYPs} + CL_{int,UGTs}} \quad (4)$$

CBD was assumed to be metabolized only by the CYPs and UGTs assessed in the current study. This assumption is justified because when the percent inhibition values were summed, minimal to no depletion remained when compared with the -NADPH or -UDPGA condition. The relative contributions of CYP and UGT isoforms to CBD metabolism were calculated using eqs. 5 and 6, respectively (Ahire et al., 2017):

$$f_{m,CYP,i} = \frac{f_{m,CYPs} \times \% \; inhibition}{sum \; of \; total \; \% \; inhibition \; across \; CYP \; isoforms \; tested} \quad (5)$$

$$f_{m,UGT,i} = \frac{f_{m,UGTs} \times \% \; inhibition}{sum \; of \; total \; \% \; inhibition \; across \; UGT \; isoforms \; tested} \quad (6)$$

where the percent inhibition of CYP or UGT isoforms in the presence of their selective inhibitors was calculated using equation eq. 7, where $k_{dep,no \; inh}$ and $k_{dep,with \; inh}$ are the k_{dep} in the absence and presence of an inhibitor, respectively.

$$\% \; Inhibition = 100 \times \frac{k_{dep,no \; inh} - k_{dep,with \; inh}}{k_{dep,no \; inh}} \quad (7)$$

PBPK Model Development and Validation. A schematic of the workflow for the development and validation of a PBPK model for CBD in healthy adult, HI adult, and pediatric populations is shown (Fig. 1). Key physicochemical, blood binding, and PK parameters used to simulate the pharmacokinetics of CBD are listed in Table 1. The predicted tissue to plasma partition coefficient (using Simcyp method 1) and steady-state volume of distribution were used to develop a whole-body CBD PBPK model (Poulin and Theil, 2002). All tissues were assumed to be perfusion-limited compartments because CBD's permeability-surface area product considerably exceeded the tissue blood flow (calculated using PK-Sim version 11; data not shown). Parenthetically, we note that CBD does not appear to be a substrate for any transporters (Epidiolex Package Insert). The liver was considered the main site of CBD metabolism because its renal clearance is negligible (Tayo et al., 2020; Epidiolex Package Insert).

To predict the hepatic CBD clearance, first, our in-house in vitro CL_{int} and f_m data (Table 2) were used i.e., bottom-up PBPK modeling (Simcyp version 20; Certara, Sheffield, UK). Because this approach considerably underestimated the intravenous CBD AUC and C_{max} (Ohlsson et al., 1986), likely due to overestimation of the in vivo hepatic CL_{int}, a middle-out modeling approach was adopted instead (Tsamandouras et al., 2015; Ladumor et al., 2019a). To do so, first CBD hepatic clearance (CL_H) was estimated from the intravenous plasma CBD clearance (CL_{IV}) (Ohlsson et al., 1986). From this estimate, the in vivo intrinsic
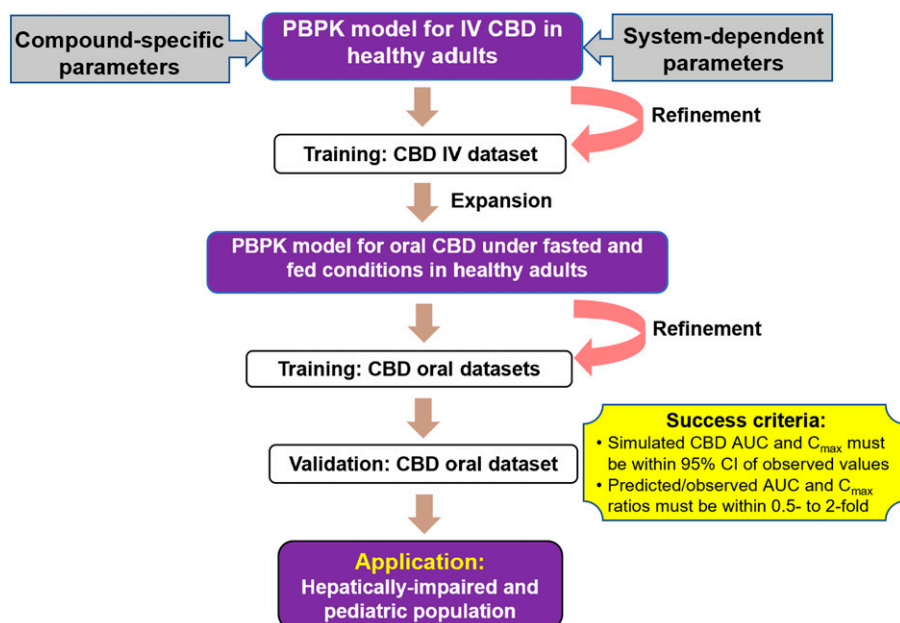
Fig. 1. Workflow for the development and validation of a PBPK model for CBD in healthy and hepatically-impaired adults and in children.

hepatic clearance ($CL_{int,H}$) was back-calculated from CL_H using the dispersion model (Supplemental Methods and Supplemental Fig. 1). Then, the in vitro $CL_{int,in\ vitro}$ of individual UGT or CYP isoforms was estimated based on their in vivo $CL_{int,H}$ (Supplemental Methods and Supplemental Fig. 1). These $CL_{int,in\ vitro}$ values were assigned to individual UGT and CYP isoforms based on their respective in vitro contribution to CBD metabolism determined in the current study. The inactivation kinetic parameters (binding-corrected half-maximal inactivation constant; $K_{I,u}$ and k_{inact}) for CYP1A2, CYP2C19, and CYP3A by CBD (Bansal et al., 2020) were included in the PBPK model to account for time-dependent inhibition of these enzymes by CBD.

The first-order absorption model was used to predict the oral CBD PK profile. The fraction of CBD absorbed (F_a) after a single oral dose of CBD administered under fasted, fed, and high-fat fed conditions was optimized (using the Parameter Estimation module of the Simcyp simulator) to recapitulate the observed CBD PK profiles of their respective training datasets. The absorption rate constant (k_a) and lag time for CBD absorption were estimated to capture the observed C_{max} and t_{max}, respectively.

Simulations were conducted using the Simcyp healthy volunteers virtual population (see Supplemental Table 1). A total of 20 trials were simulated to mimic the population variability in the observed data. The number of subjects, their age, sex distribution, CBD dose, dosing regimen, dose units, route of administration, and prandial state in the simulations were identical to those in the corresponding in vivo study.

Model predictive performance was evaluated by comparing the simulated AUC and C_{max} to the observed in vivo data that were not used as a training dataset. The model was considered validated if the predicted AUC and C_{max} fell within the 95% confidence interval (CI) of the observed values and the ratio of predicted to observed PK endpoints was within the 0.5- to 2-fold range. Additionally, the simulated concentration-time profiles were visually compared with the observed digitized in vivo data (WebPlotDigitizer) (https://automeris.io/WebPlotDigitizer/).

PBPK Model Validation in HI Adult Populations. After developing and validating a base PBPK model for predicting CBD systemic exposure after single-dose administration in healthy adults under fed conditions, this model was further validated in HI adult populations. Existing Simcyp models for mild (Child-Pugh A), moderate (Child-Pugh B), and severe (Child-Pugh C) hepatic impairment were used to predict CBD systemic exposure in HI populations. Although the Simcyp version 20 model incorporates the decrease in CYP protein abundance and other physiologic changes resulting from hepatic impairment, changes in UGT protein abundance are not incorporated. Given that UGT1A9 protein abundance (picomoles per milligram of microsomal protein) decreases by 40% and 64%, respectively, in moderate and severe HI patients relative to healthy subjects and that

UGT2B7 protein abundance decreases by 25%, 55% and 80% in mild, moderate, and severe HI subjects, respectively, relative to healthy subjects (El-Khateeb et al., 2021), UGT1A9 or UGT2B7-mediated CL_{int} was modified using eq. 8 (Prasad et al., 2018; Ahire et al., 2022):

$$CL_{int,UGTi\ (HI)} = CL_{int,UGTi\ (control)} \times \frac{Abundance_{UGTi\ (HI)}}{Abundance_{UGTi\ (control)}} \quad (8)$$

PBPK Model Validation in Pediatric Populations. The base PBPK model for predicting the systemic exposure to oral CBD administered under fed conditions in adult populations was applied to the pediatric population, ages 4–10 years using the Simcyp pediatric model. Simcyp default ontogeny profiles for CYPs and UGTs, except UGT2B7, were used because UGT2B7 ontogeny has not been incorporated in Simcyp version 20. Therefore, reported UGT2B7 ontogeny data were included to predict CBD systemic exposure in children (Bhatt et al., 2019). The model was populated with the CBD CYP inactivation kinetic parameters ($K_{I,u}$ and k_{inact}) to capture the accumulation and time-dependent inhibition of enzymes after multiple oral doses of CBD administration. CBD accumulation ratio was calculated as the ratio of CBD AUC_{0-5h} after the last dose and after a single dose (because the AUC after the first dose was not available). Because the latter was not available for all single doses (i.e., 2.5, 5, or 10 mg/kg), it was estimated from the observed AUC_{0-5h} after a single 1.25 mg/kg dose assuming dose proportionality. The CBD pediatric population model was considered validated if the success criteria specified for the base model were met.

Results

Determination of Intrinsic Clearance and Fraction Metabolized. CYP- or UGT-mediated CBD depletion rates were higher at 50 nM compared with 1 μM (data not shown), which was likely due to auto-inhibition at 1 μM. Therefore, all subsequent CBD depletion experiments were conducted at 50 nM. CBD depletion could not be monitored at <50 nM due to assay detection limitations. UGT-mediated CL_{int} for CBD was 3.5-fold higher than the CYP-mediated CL_{int} (Table 2). Based on CL_{int}, UGTs contributed 80% to CBD depletion (Fig. 2; Table 2). UGT-mediated depletion of CBD was inhibited most (82%) by the UGT2B7 inhibitor, β-phenyllongifolol (Fig. 2B). A UGT1A9 inhibitor, digoxin, inhibited CBD depletion by 21%. Unlike UGTs, CYPs contributed modestly (20%) to CBD metabolism (note that a 6-fold higher concentration of HLM was used to quantify CYP- versus UGT-mediated CBD depletion) (Fig. 2). CYP-mediated depletion of CBD was inhibited 47% and 41% by azamulin

TABLE 1

Drug and system-specific input parameters for the development of a physiologically based pharmacokinetic model for cannabidiol using Simcyp v20

	Parameter	Value(s) or model	Reference
Physicochemical and plasma binding	Molecular weight (g/mol)	314.5	ChEMBL
	log P	6.33	ChEMBL
	pK_a	9.13	ChEMBL
	B/P	0.67	(Samara et al., 1988)
	$f_{u,p}$	0.013	(Bansal et al., 2022)
Absorption	Absorption model	First-order absorption	
	f_a	0.25^a, 0.45^b, 0.74^c	Estimated by optimization[#]
	k_a (1/h)	0.55^a, $1^{b,c}$	Estimated by optimization*
	lag time (h)	$1.5^{a,b,c}$	Estimated by optimization*
	$f_{u,gut}$	0.013	Assumed same as $f_{u,p}$
Distribution	Distribution model	Full PBPK	Simcyp Method 1
	V_{ss} (L/kg)	16.64	Predicted
Elimination	CL_{IV} (L/h)	54	(Ohlsson et al., 1986)
	f_e (CL_R in L/h)	0 (0)	(Tayo et al., 2020)
	f_m (CL_H in L/h)	1 (54)	(Ohlsson et al., 1986)
	Metabolic clearance	Dispersion model	(Roberts and Rowland, 1986)
	$CL_{int,H}$ (μl/min/mg)	3400	Back-calculated from IV data
	$f_{m,UGT}$	0.795	Determined experimentally
	$f_{m,UGT1A9}$	0.159	Determined experimentally
	$f_{m,UGT2B7}$	0.636	Determined experimentally
	$f_{m,CYP}$	0.205	Determined experimentally
	$f_{m,CYP1A2}$	0.016	Determined experimentally
	$f_{m,CYP2B6}$	0.014	Determined experimentally
	$f_{m,CYP2C8}$	0.015	Determined experimentally
	$f_{m,CYP2C9}$	0.037	Determined experimentally
	$f_{m,CYP2C19}$	0.057	Determined experimentally
	$f_{m,CYP2D6}$	0.011	Determined experimentally
	$f_{m,CYP3A4}$	0.065	Determined experimentally
	$CL_{int,UGT}$ (μl/min/mg)	2703	Determined by middle-out approach
	$CL_{int,UGT1A9}$ (μl/min/mg)	541	Determined by middle-out approach
	$CL_{int,UGT2B7}$ (μl/min/mg)	2162	Determined by middle-out approach
	$CL_{int,CYP}$ (μl/min/mg)	697	Determined by middle-out approach
	$CL_{int,CYP1A2}$ (μl/min/mg)	56	Determined by middle-out approach
	$CL_{int,CYP2B6}$ (μl/min/mg)	46	Determined by middle-out approach
	$CL_{int,CYP2C8}$ (μl/min/mg)	51	Determined by middle-out approach
	$CL_{int,CYP2C9}$ (μl/min/mg)	93	Determined by middle-out approach
	$CL_{int,CYP2C19}$ (μl/min/mg)	193	Determined by middle-out approach
	$CL_{int,CYP2D6}$ (μl/min/mg)	38	Determined by middle-out approach
	$CL_{int,CYP3A4}$ (μl/min/mg)	220	Determined by middle-out approach
Auto-inhibition	CYP1A2 inactivation		(Bansal et al., 2020)
	$K_{I,u}$ (μM)	0.020	
	k_{inact} (1/h)	4.2	
	CYP2C19 inactivation		
	$K_{I,u}$ (μM)	0.073	
	k_{inact} (1/h)	2.4	
	CYP3A inactivation		
	$K_{I,u}$ (μM)	0.106	
	k_{inact} (1/h)	4.7	

Abbreviations: B/P, blood to plasma concentration ratio; CL_H, hepatic clearance; CL_R, renal plasma clearance; f_e, fraction of drug cleared unchanged in the urine, f_m, fraction of drug cleared through hepatic metabolism; $f_{u,gut}$, unbound fraction in the gut; $f_{u,p}$, unbound fraction in plasma; $K_{I,u}$, binding-corrected half-maximal inactivation concentration; logP, partition coefficient; pKa, dissociation constant.
[a]Fasted, [b]Fed, [c]High-fat fed.
[#]F_a was optimized using the Parameter Estimation module of the Simcyp simulator.
*Parameters were optimized to recapitulate the observed CBD pharmacokinetic profiles.

(CYP3A inhibitor) and benzylnirvanol (CYP2C19 inhibitor), respectively (Fig. 2A). Sulfaphenazole (CYP2C9 inhibitor) inhibited CBD depletion by 20%, and other CYP isoform inhibitors, including furafylline (CYP1A2), 2-PPP (CYP2B6), montelukast (CYP2C8), and quinidine (CYP2D6), inhibited CBD depletion by <12% (Fig. 2A).

PBPK Model for CBD after Intravenous Administration. The PBPK model-predicted CBD plasma concentration-time profile following intravenous administration was comparable to the observed in vivo data used as a training dataset (Fig. 3). Most of the data points (>90%) were within the 5th–95th percentile of the virtual population. The predicted CBD AUC was within the 95% CI of the observed value (Table 3). The predicted to observed AUC ratio was 1.16. These results indicated successful development of a PBPK model for CBD following intravenous administration.

PBPK Model for CBD after Oral Administration. The model-predicted CBD plasma PK profiles following oral administration under

fasted, fed, and high-fat fed conditions were comparable to the observed in vivo data (Fig. 4). All observed data points fell within the 5th–95th percentile of the virtual population. The predicted CBD AUC and C_{max} were within the 95% CI of the observed values (Table 3). The predicted to observed AUC and C_{max} ratios were within the range 0.84–1.19. Simcyp-estimated fraction of CBD escaping the gut was similar (85–90%) under the fasted or fed conditions. In contrast, Simcyp-estimated fraction of CBD escaping the liver (F_h) was 1.5-fold higher under fed conditions (47%) compared with the fasted condition (31%). After developing these PBPK models (fasted, fed, and high-fat meal), model predictive performance was evaluated using multiple validation datasets that were not used for model-training. The PBPK models were validated as evidenced by the predicted AUC falling within the 95% CI of the observed value (Table 3). However, CBD F_a required refining to accurately predict systemic exposure following higher CBD doses [3000 mg

TABLE 2

Mean $CL_{int,u}$ and f_m values for CBD depletion by CYP or UGT isoforms estimated using pooled HLMs

Enzyme	Isoform	Selective inhibitor	$CL_{int,u}$ ($\mu l/min/mg$)[a]	Relative contribution (f_m)[a]
CYP			14967	0.21
	CYP1A2	Furafylline	1200	0.016
	CYP2B6	2-PPP: 2-phenyl-2-(1-piperidinyl)propane	1000	0.014
	CYP2C8	Montelukast	1100	0.015
	CYP2C9	Sulfaphenazole	2000	0.027
	CYP2C19	Benzylnirvanol	4133	0.057
	CYP2D6	Quinidine	800	0.011
	CYP3A	Azamulin	4734	0.065
UGT			57867	0.79
	UGT1A9	Digoxin	11567	0.159
	UGT2B7	β-Phenyllongifolol	46300	0.636

[a]Estimated from two independent experiments, each conducted in duplicate. The unbound $CL_{int,u}$ was calculated using the reported fraction unbound in incubation containing HLM and bovine serum albumin ($f_{u,inc}$ = 0.03) for CBD (Bansal et al., 2022).

(F_a = 0.2), 4500 mg (F_a = 0.17), or 6000 mg (F_a = 0.15)] in the fasted condition (Fig. 5). The predicted to observed AUC and C_{max} ratios for the validation datasets were within the range 0.79–1.50. Model-predicted half-life of CBD was also comparable to the observed value (50–60 hours) based on CBD plasma sampling for 8 days (Perkins et al., 2020).

Oral CBD PBPK Model Validation in HI and Pediatric Populations. In mild, moderate, and severe HI populations, using the Simcyp version 20 default HI model, the predicted to observed CBD C_{max} ratio was within acceptable limits (greater than 0.5-fold). The predicted CBD AUC after a single oral dose of CBD in HI populations, except for the severe HI population, fell within the acceptance criteria (Table 4). After incorporating the altered UGT1A9 and 2B7 protein abundance in mild, moderate, and severe HI populations, model performance improved (Table 4), especially in severe HI populations, and all observed data points fell within the 5th–95th percentile of the virtual HI populations (Fig. 6). Simcyp-estimated half-life of CBD increased by 2-fold in mild HI patients and by threefold in moderate and severe HI patients, which is comparable to the observed values (Taylor et al., 2019). Hepatic impairment was predicted to have no effect on CBD t_{max}, which is consistent with the observed data (Taylor et al., 2019).
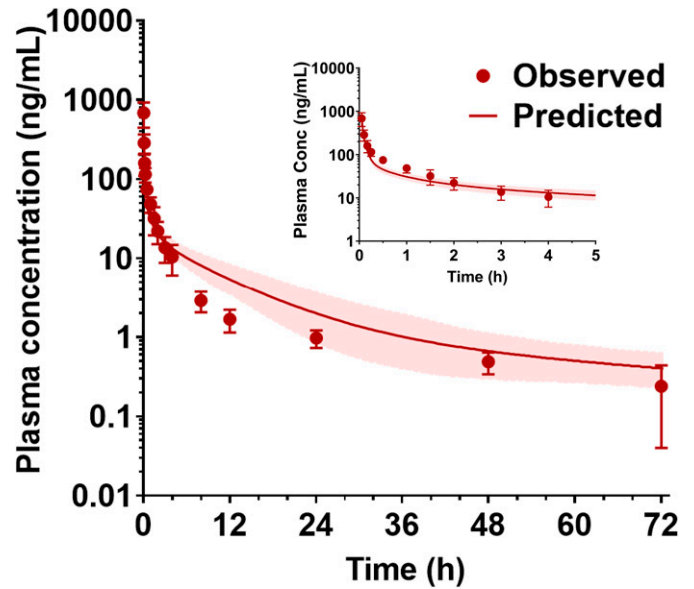

Fig. 3. PBPK model-predicted and observed CBD plasma PK profile after intravenous (20 mg) administration to healthy adults. Data are observed mean values (±S.D.) (Ohlsson et al., 1986), and red line represents the PBPK model-predicted CBD-plasma concentration-time profile. The shaded area represents the 5th–95th percentile of the virtual population. The inset is the PBPK model-predicted and observed CBD plasma PK profile from 0–5 hours. The model-predicted AUC lay within the 95% CI of the observed data, and the ratio of predicted to observed AUC was within the 0.5- to 2-fold range (Table 3).

Model performance was also validated in the pediatric population, in which CBD AUC and C_{max} after single- and multiple-dose oral administration fell within the pre-defined acceptance criteria (Table 5). The predicted CBD accumulation ratio after multiple-dose administration was within the 0.5- to 2-fold range (Table 5). Incorporating ontogeny of UGT2B7 in the Simcyp-default model for children had minimal effect on CBD AUC and C_{max} (data not shown).

Discussion

This study determined the relative contribution of UGT and CYP isoforms to CBD depletion by HLMs using in vitro reaction phenotyping. We found that UGTs (UGT1A9/2B7, 80%), rather than CYPs (20%), are the major contributors to CBD metabolism. These observations are
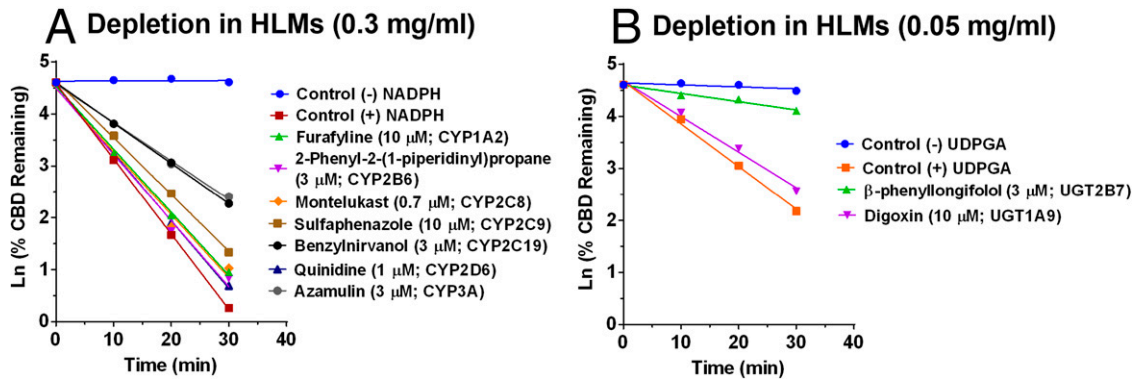

Fig. 2. Cannabidiol (CBD; 50 nM) reaction phenotyping using pooled HLMs (A) 0.3 mg/ml + NADPH or (B) 0.05 mg/ml + UDPGA in the presence or absence of (A) CYP or (B) UGT selective inhibitors. The estimated intrinsic clearance (Table 2) for CBD indicated that UGTs are the major contributors to CBD metabolism. Of these, UGT2B7 is the major contributor (β-phenyllongifolol inhibited UGT-mediated depletion of cannabidiol by the greatest extent). CYP2C19 and CYP3A are the major CYPs responsible for CYP-mediated CBD depletion because the CYP-selective inhibitors tested, benzylnirvanol (CYP2C19) and azamulin (CYP3A), inhibited depletion by the greatest extent. Solid lines represent the % remaining predicted by using linear regression (GraphPad Prism 6.01). Data are from a representative experiment of two independent experiments, each conducted in duplicate. Note: the HLM concentration used for CYP-depletion studies (A) was 6-fold higher than that used for UGT-depletion studies (B).

TABLE 3

PBPK model-predicted and observed (mean and 95% CI) cannabidiol CBD exposure in healthy adults after a single intravenous or oral dose of CBD

Dataset	#	#F	Age (SD)	Prandial state	Dose (Route)	Parameter	Obs	95% CI	Pred	Pred/Obs
A1[a]	5	0	19–33	Fasted	20 mg (Intravenous infusion)	$AUC_{(0-t)}$ (ng*h/ml)	311	231–419	362	1.16
A2[b]	12	8	25 (6)	Fasted	1500 mg (Oral)	$AUC_{(0-t)}$ (ng*h/ml)	1987	1495–2640	1740	0.88
						$AUC_{(0-\infty)}$ (ng*h/ml)	2198	1697–2847	1960	0.89
						C_{max} (ng/ml)	335	224–502	282	0.84
A3	6	5	26 (3)	Fasted	1500 mg (Oral)	$AUC_{(0-t)}$ (ng*h/ml)	1517	873–2637	1761	1.16
						$AUC_{(0-\infty)}$ (ng*h/ml)	1618	950–2755	2028	1.25
						C_{max} (ng/ml)	292	160–536	299	1.02
A4	6	3	25 (5)	Fasted	3000 mg (Oral)	$AUC_{(0-t)}$ (ng*h/ml)	2669	2013–3540	2789	1.04
						$AUC_{(0-\infty)}$ (ng*h/ml)	2802	2130–3686	3127	1.12
						C_{max} (ng/ml)	533	406–700	455	0.85
A5	6	6	26 (8)	Fasted	4500 mg (Oral)	$AUC_{(0-t)}$ (ng*h/ml)	3215	2199–4701	3707	1.15
						$AUC_{(0-\infty)}$ (ng*h/ml)	3426	2375–4942	4324	1.26
						C_{max} (ng/ml)	722	487–1070	633	0.88
A6	6	4	23 (3)	Fasted	6000 mg (Oral)	$AUC_{(0-t)}$ (ng*h/ml)	3696	2106–6485	4283	1.16
						$AUC_{(0-\infty)}$ (ng*h/ml)	3900	2230–6820	4867	1.25
						C_{max} (ng/ml)	782	438–1396	708	0.91
A7[c]	8	4	58 (8)	Fed	200 mg (Oral)	$AUC_{(0-t)}$ (ng*h/ml)	449	285–708	385	0.86
						$AUC_{(0-\infty)}$ (ng*h/ml)	474	300–749	430	0.91
						C_{max} (ng/ml)	148	98–223	119	0.80
A8	8	5	60 (12)	Fed	200 mg (Oral)	$AUC_{(0-t)}$ (ng*h/ml)	464	288–747	412	0.89
						$AUC_{(0-\infty)}$ (ng*h/ml)	499	312–799	453	0.91
						C_{max} (ng/ml)	153	96–243	121	0.79
A9[d]	6	1	25 (6)	High-fat	10 mg/kg (Oral)	$AUC_{(0-t)}$ (ng*h/ml)	4025	3022–5361	3299	0.82
						$AUC_{(0-\infty)}$ (ng*h/ml)	4227	3174–5630	3416	0.81
						C_{max} (ng/ml)	626	409–957	748	1.19
A10	6	2	26 (5)	High-fat	5 mg/kg (Oral)	$AUC_{(0-t)}$ (ng*h/ml)	1793	1461–2200	1591	0.89
						$AUC_{(0-\infty)}$ (ng*h/ml)	1905	1564–2320	1647	0.86
						C_{max} (ng/ml)	248	144–428	370	1.49
A11	6	1	23 (7)	High-fat	20 mg/kg (Oral)	$AUC_{(0-t)}$ (ng*h/ml)	7618	6115–9491	6683	0.88
						$AUC_{(0-\infty)}$ (ng*h/ml)	8008	6379–10053	6923	0.86
						C_{max} (ng/ml)	1003	665–1513	1505	1.50

[a]Training dataset used for CBD intravenous PBPK model development.
[b]Dataset used for training the PBPK model for CBD after oral administration under fasted conditions. This data set was chosen over other available data sets because of its longer sampling duration.
[c]Dataset used for training the PBPK model for CBD after oral administration under fed conditions.
[d]Dataset used for training the PBPK model for CBD after oral administration under high-fat fed conditions.
Dataset A1 is from Ohlsson et al., 1984, A2-A6 from Taylor et al., 2018, A7 from Taylor et al., 2019, A8 from Tayo et al., 2019, and A9-A11 from Perkin et al., 2020.
F, Female; Obs: Observed data; Pred: Predicted data.

consistent with results from an in vivo study showing that itraconazole, a potent CYP3A inhibitor, altered the AUC and C_{max} of CBD by <10%, whereas fluconazole, a CYP2C19 inhibitor, increased CBD AUC and C_{max} by 22–24% (Epidiolex Package Insert). Moreover, rifampin, a CYP3A and CYP2C19 inducer, decreased CBD AUC and C_{max} by <30% (Epidiolex Package Insert). In contrast, a previous
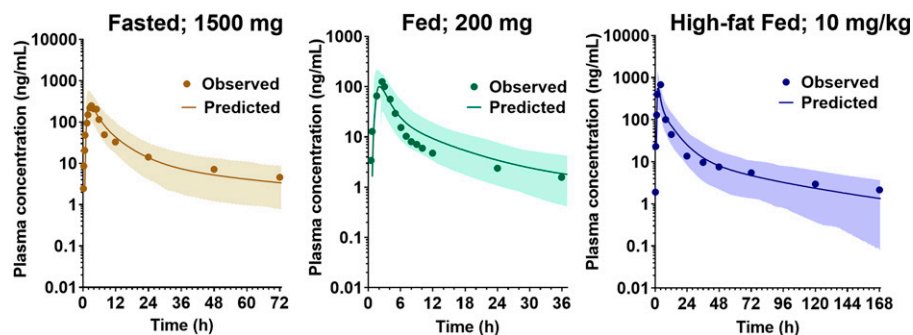

Fig. 4. PBPK model-predicted and observed CBD plasma PK profiles after oral administration (fasted, fed, and high-fat fed condition) to healthy adults. A first-order absorption model was used to predict the CBD PK profiles; F_a was optimized using the Parameter Estimation module of the Simcyp simulator and k_a was optimized to recapitulate the observed CBD PK profiles. Data points are the observed mean values, and the line represents the model-predicted CBD PK profile. The shaded area represents the 5th-95th percentile of the virtual population. The predicted AUC and C_{max} were within the 95% CI of the observed values, and the ratio of predicted to observed AUC and C_{max} were within 0.5- to 2-fold range (Table 3).
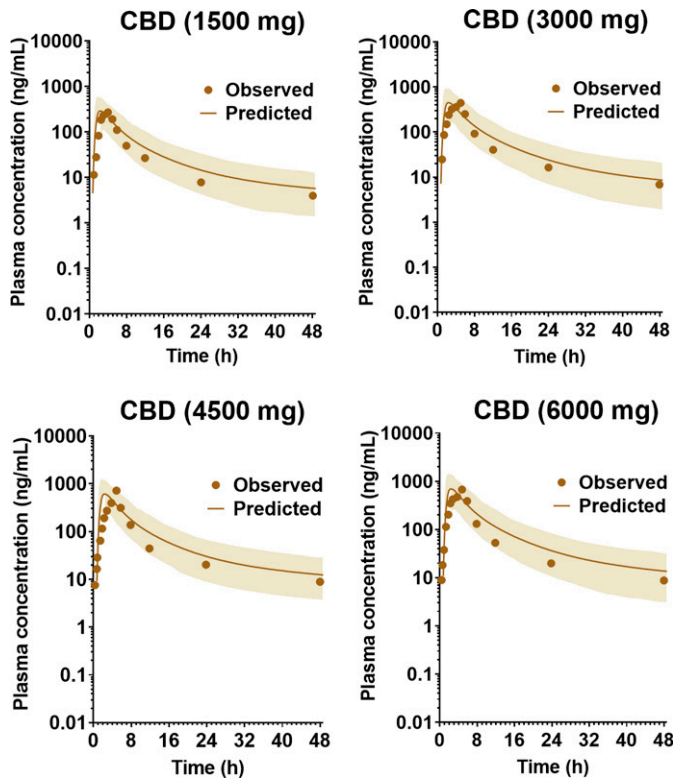
Fig. 5. PBPK model-predicted and observed CBD plasma PK profiles after oral administration of ascending doses of CBD administered to healthy adults under fasting conditions. The predicted AUC and C_{max} fell within the 95% CI of the observed value and the ratio of the predicted and observed AUC and C_{max} were within 0.5- to 2-fold range (see Table 3). F_a was optimized to recapitulate the observed dose-dependent CBD PK profiles. Data points are the observed mean values, and the line represents model-predicted CBD-plasma concentration-time profile. Shaded area represents the 5th–95th percentile of the virtual population.

in vitro CBD (1 μM) depletion study involving HLMs concluded that CYPs, rather than UGTs, are the major enzymes that metabolize CBD (Beers et al., 2021). Given that CBD is a more potent inhibitor of UGT2B7 and UGT1A9 (Bansal et al., 2021) than CYPs (Bansal et al., 2020), such contradictory results are likely due to auto-inhibition of UGT-mediated metabolism of CBD at the 1 μM concentration used in that study. Nevertheless an in vivo study with UGT inhibitors is needed to confirm whether the UGTs are the major contributors to CBD clearance.

Using the contributions by UGTs and CYPs, we used PBPK modeling and simulation to simulate CBD PK profiles in healthy adults under

fasted and fed conditions. The model was trained and validated for healthy adults. To do so, first, we used a bottom-up approach, which overestimated (by 21-fold) CBD in vivo CL_{int}, indicating that HLMs do not fully capture hepatic metabolism in vivo, perhaps because intracellular proteins, such as fatty acid-binding proteins, may hinder access of CBD to the enzymes (Elmes et al., 2015). Therefore, we used a middle-out approach to build the CBD PBPK model (Tsamandouras et al., 2015; Ladumor et al., 2019a). CBD CL_{IV} was determined in a single study in which deuterated CBD (20 mg) was administered as an intravenous infusion to five subjects (Ohlsson et al., 1986). Given that CBD half-life is approximately 50–60 hours (Epidiolex Package Insert), this CL_{IV} is likely overestimated because the AUC was calculated over one half-life (48 hours) in 2 subjects and 1.5 half-lives (78 hours) in three subjects. Therefore, we used the lower limit of the 90% CI (54 L/h) of the observed CL_{IV} (70 L/h) to predict the CBD PK. Given that the renal clearance of CBD is minimal (Tayo et al., 2020), the blood clearance of CBD was estimated to be approximate liver blood flow deeming CBD a high extraction ratio drug (>0.70). Therefore, the dispersion model was chosen to back-calculate CBD in vitro CL_{int} from in vivo CL_{IV} (Yamamoto et al., 2005). Next, based on the individual CYP and UGT enzymes contributing to CBD metabolism in our depletion studies, CBD CL_{int} was segregated into fractions contributed by each of the identified CYPs and UGTs.

Due to the low aqueous solubility of CBD in intestinal fluid, which can result in poor and large inter-individual variability in absorption, the oral CBD PK datasets were obtained from studies in which the drug was administered in sesame or soybean oil and/or alcohol. Nevertheless, under fasting conditions, CBD systemic exposure is less than proportional with an increase in dose (Table 3; Fig. 5) (Taylor et al., 2018). Therefore, we optimized F_a for the higher CBD doses administered under fasting conditions (3000, 4500, and 6000 mg). In contrast, under high-fat fed conditions, CBD exposure increases linearly with dose (Fig. 6) (Perkins et al., 2020), demonstrating CBD dose-independent kinetics (including Fa). Under both fed and fasted conditions, the estimated fraction of CBD escaping the gut suggests minimal intestinal CBD metabolism. However, we estimated a higher F_h under fed versus fasting conditions, which was likely due to the higher splanchnic blood flow under fed conditions (Rose et al., 2017). The model-predicted oral bioavailability of CBD was 7%, 17%, and 30% under fasted, fed, and high-fat fed condition, respectively, which is comparable to the corresponding observed oral bioavailability (8%, 16%, and 30%) that was calculated by comparing CBD AUC following oral and intravenous administration (Ohlsson et al., 1986; Taylor et al., 2018, 2019; Perkins et al., 2020; Tayo et al., 2020). The PBPK model-predicted CBD AUC

TABLE 4

PBPK model-predicted and observed (mean and 95% CI) CBD exposure in HI subjects after a single oral dose (200 mg) of CBD administered under the fed condition

Dataset	Population Type	#	#F	Age (SD)	Parameter	Obs	95% CI	Pred1[a]	Pred2[b]	Pred1/Obs	Pred2/Obs
H1	Mild HI	8	4	56	$AUC_{(0-t)}$ (ng*h/ml)	648	484–868	491	550	0.76	0.85
				(11)	$AUC_{(0-\infty)}$ (ng*h/ml)	699	522–937	543	611	0.78	0.87
					C_{max} (ng/ml)	233	150–362	132	143	0.57	0.61
H2	Moderate HI	8	3	53	$AUC_{(0-t)}$ (ng*h/ml)	1054	813–1367	927	1396	0.88	1.32
				(7)	$AUC_{(0-\infty)}$ (ng*h/ml)	1163	891–1518	1032	1616	0.89	1.39
					C_{max} (ng/ml)	354	267–469	218	262	0.62	0.74
H3	Severe HI	6	3	55	$AUC_{(0-t)}$ (ng*h/ml)	1855	1254–2744	1000	2178	0.54	1.17
				(10)	$AUC_{(0-\infty)}$ (ng*h/ml)	2439	1893–3142	1119	2750	0.46	1.13
					C_{max} (ng/ml)	381	257–564	250	348	0.66	0.91

[a]Simcyp-default model.
[b]The decrease in UGT1A9 and UGT2B7 protein abundance in HI was integrated into Simcyp-default model for mild, moderate, and severe HI populations.
Datasets H1-H3 are from Taylor et al., 2019.
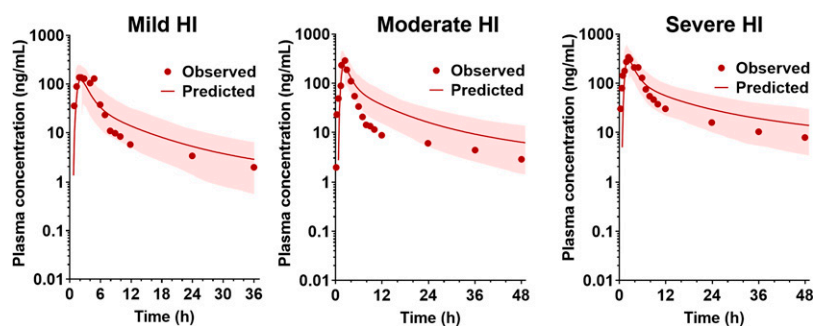F, Female; Obs, Observed data; Pred, Predicted data.

Fig. 6. PBPK model-predicted and observed CBD (200 mg) plasma PK profiles after oral administration to HI patients. Our PBPK model for CBD in HI populations was validated as evidenced by the predicted AUC and C_{max} falling within the 95% CI of the observed values and the ratios of predicted and observed AUC and C_{max} falling within 0.5- to 2-fold range for multiple validation datasets (see Table 4). Simcyp Child-Pugh A, B, and C models were used to predict CBD PK in mild, moderate, and severe HI patients, respectively. The Simcyp Child-Pugh C model significantly underpredicted CBD AUC and C_{max} in severe HI patients. However, the predicted profile shown here significantly improved after integrating the 64% and 80% decrease in UGT1A9 and UGT2B7 protein abundance, respectively, (measured by quantitative targeted proteomics) observed in these subjects (Table 4) (El-Khateeb et al., 2021). Data points are the observed mean values, and the line represents model-predicted CBD-plasma concentration-time profile. Shaded area represents the 5th–95th percentile of the virtual population.

and C_{max} after single oral dose administration fell within the pre-defined acceptance criteria (Table 3; Figs. 4 and 5). These model validation results indicate successful development of a PBPK model to predict CBD PK under fasted and fed conditions.

To evaluate optimal drug dosing regimens in HI patients, regulatory agencies recommend conducting PK studies in this population for drugs metabolized extensively in the liver (Heimbach et al., 2021). This recommendation is based on hepatic impairment being associated with alterations in hepatic drug metabolizing enzyme abundance (CYPs and UGTs) and changes in drug plasma protein binding (Verbeeck, 2008; Ladumor et al., 2019b; Sharma et al., 2020). Although Simcyp (V20) incorporates changes in CYP abundance in the liver and intestine for different degrees of hepatic impairment, such changes in UGT abundance are not incorporated. After incorporating changes in UGT1A9 and 2B7 abundances in mild, moderate, and severe hepatic impairment (El-Khateeb et al., 2021), our PBPK model recapitulated the observed increase in CBD AUC in patients with differing degrees of severity (mild, moderate, and severe) (Table 4). Accordingly, we propose that this CBD PBPK model could be applied to predict the magnitude of CBD-drug interactions in HI adults. Parenthetically, Qian et al. have published a PBPK model for CBD, but they did not account for the contribution of UGTs to CBD metabolism (Qian and Markowitz, 2022).

Pediatric PBPK models are commonly used to guide pediatric dose selection, as well as design, reduce, or replace in vivo PK studies in this population (Johnson et al., 2021). In the current study, a PBPK model was developed that successfully predicted AUC and C_{max} in children aged 4–10 years, as evidenced by both endpoints lying within our pre-defined acceptance criteria (Table 5; unfortunately, the AUC profiles of CBD are not published and therefore we could not compare the predicted profiles with the observed). Our model also successfully predicted CBD accumulation after multiple-dose administration (Table 5). The model-predicted CBD accumulation ratio (1.4–1.5) in children was comparable to that in adults. Moreover, because CYPs play a minor role in CBD clearance (Table 2), their inactivation by CBD played a minimal role in CBD accumulation. The estimated F_h in this population was 1.55-fold higher than that in adults, whereas the in vivo plasma CL (35 L/h) was 63% of adults, demonstrating the effect of the mass of microsomal protein per liver weight, tissue weight, protein binding, and enzyme ontogeny in this population. Per the Simcyp model, UGT2B7 abundance in children increases linearly with age, reaching that in adults at 21 years of age; this trajectory is not supported by experimental data (incorporated in our model) showing that UGT2B7 protein abundance reaches 50% of the adult value at 2.6 years of age (Bhatt et al., 2019). However, incorporating these ontogeny data in our pediatric PBPK

TABLE 5

PBPK model-predicted and observed (mean and 95% CI) CBD exposure in pediatric subjects (4–10 years) after a single or multiple oral doses of CBD administered under the fed condition

Dataset	#	#F	Dose	Parameter	Observed	95% CI	Predicted	Predicted/Observed
PD1	8	5	1.25 mg/kg (Single dose)	AUC$_{(0-t)}$ (ng*h/ml)[a]	73.7	33–134	105	1.42
				C_{max} (ng/ml)	37.6	20–60	44	1.17
PD2	10	5	2.5 mg/kg bid	AUC$_{(0-t)}$ (ng*h/ml)[a]	241	139–417	301	1.25
				C_{max} (ng/ml)	130	70–241	109	0.83
				Accumulation ratio	1.64[b]		1.43[c]	0.87
PD3	7	5	5 mg/kg bid	AUC$_{(0-t)}$ (ng*h/ml)[a]	722	429–1215	614	0.85
				C_{max} (ng/ml)	242	155–377	222	0.92
				Accumulation ratio	2.45[b]		1.46[c]	0.60
PD4	7	5	10 mg/kg bid	AUC$_{(0-t)}$ (ng*h/ml)[a]	963	536–1732	1244	1.29
				C_{max} (ng/ml)	380	208–696	450	1.18
				Accumulation ratio	1.63[b]		1.48[c]	0.91

[a]AUC$_{0-t}$ from 0 to 5 h after a single or the last dose.
[b]The ratio of CBD AUC from 0 to 5 h after the last dose and after a single dose (the AUC after first dose was not available). CBD AUC from 0 to 5 h after a single dose (2.5, 5, or 10 mg/kg) was not available, therefore it was estimated from the observed AUC from 0 to 5 h after a single dose of 1.25 mg/kg assuming dose proportionality.
[c]Calculated in the same way as the observed accumulation ratio.
Datasets PD1–PD4 data are from Devinsky et al., 2018. PD1 data are after single dose of CBD and PD2, PD3, and PD4 data are for multiple dose administration of CBD.
F, Female.

model had minimal effect on CBD AUC and $C_{max.}$ In contrast, CYP abundance in children aged 4–10 years is comparable to that in adults. This pediatric CBD PBPK model can now be extrapolated to predict CBD exposure in children outside the 4–10 year age range. The model can also be applied to predict the magnitude of CBD-drug interactions, as other anti-epileptic drugs are often prescribed with CBD (Devinsky et al., 2018b).

Our study has several limitations. First, we could not validate our PBPK model with an independent intravenous dataset because such data are not available. Second, due to limited information about CBD in vivo intestinal solubility, bile-partition coefficient, supersaturation ratio, and precipitation rate constant, we could not use the mechanistic advanced dissolution, absorption, and metabolism (ADAM) model to capture the dose-dependent CBD F_a and positive food effect on F_a. Therefore, we used a first-order model for CBD absorption. Third, we could validate our model with multiple dosing in children but not in healthy adults due to the unavailability of such data. However, the observed CBD AUC in children after a single or last dose was determined from 0 to 5 hours, which is not considered an ideal validation dataset or one that can be used to estimate the accumulation ratio. Last, our pediatric PBPK model did not incorporate some physiologic development changes, including changes in small intestinal length, which can affect CBD absorption in pediatric populations (Johnson et al., 2018).

In conclusion, we showed that CBD is cleared from the body predominantly by hepatic UGT2B7- and UGT1A9-mediated metabolism (f_m ~0.8). In addition, we incorporated UGT and CYP contributions to CBD metabolism in a PBPK model for CBD following intravenous and oral dosing under fasting and fed conditions. This model was applied to successfully predict CBD PK in two special populations: HI adults and children. This model can now be used to predict CBD-drug, CBD-disease, and CBD-drug-disease interaction in healthy adults and children of all ages.

Data Availability

All the data supporting the findings of this study are available within the paper and its Supplemental Data.

Authorship Contributions

Participated in research design: Bansal, Ladumor, Unadkat.
Conducted experiments: Bansal, Ladumor.
Performed data analysis: Bansal, Ladumor.
Wrote or contributed to the writing of the manuscript: Bansal, Ladumor, Paine, Unadkat.

References

Ahire D, Kruger L, Sharma S, Mettu VS, Basit A, and Prasad B (2022) Quantitative Proteomics in Translational Absorption, Distribution, Metabolism, and Excretion and Precision Medicine. *Pharmacol Rev* 74:769–796.

Ahire D, Sinha S, Brock B, Iyer R, Mandlekar S, and Subramanian M (2017) Metabolite Identification, Reaction Phenotyping, and Retrospective Drug-Drug Interaction Predictions of 17-Deacetylnorgestimate, the Active Component of the Oral Contraceptive Norgestimate. *Drug Metab Dispos* 45:676–685.

Bansal S, Maharao N, Paine MF, and Unadkat JD (2020) Predicting the Potential for Cannabinoids to Precipitate Pharmacokinetic Drug Interactions Via Reversible Inhibition or Inactivation of Major Cytochromes P450. *Drug Metab Dispos* 48:1008–1017.

Bansal S, Paine M, and Unadkat J (2021) Can cannabinoids precipitate UGT-mediated drug interactions? *FASEB J* 35:1–1.

Bansal S, Paine MF, and Unadkat JD (2022) Comprehensive Predictions of Cytochrome p450 (p450)-Mediated In Vivo Cannabinoid-Drug Interactions Based on Reversible and Time-Dependent p450 Inhibition in Human Liver Microsomes. *Drug Metab Dispos* 50:351–360.

Beers JL, Fu D, and Jackson KD (2021) Cytochrome p450-Catalyzed Metabolism of Cannabidiol to the Active Metabolite 7-Hydroxy-Cannabidiol. *Drug Metab Dispos* 49:882–891.

Bhatt DK, Mehrotra A, Gaedigk A, Chapa R, Basit A, Zhang H, Choudhari P, Boberg M, Pearce RE, Gaedigk R et al. (2019) Age- and Genotype-Dependent Variability in the Protein Abundance and Activity of Six Major Uridine Diphosphate-Glucuronosyltransferases in Human Liver. *Clin Pharmacol Ther* 105:131–141.

Bichlmaier I, Kurkela M, Joshi T, Siiskonen A, Rüffer T, Lang H, Finel M, and Yli-Kauhaluoma J (2007) Potent inhibitors of the human UDP-glucuronosyltransferase 2B7 derived from the sesquiterpenoid alcohol longifolol. *ChemMedChem* 2:881–889.

Devinsky O, Marsh E, Friedman D, Thiele E, Laux L, Sullivan J, Miller I, Flamini R, Wilfong A, Filloux F et al. (2016) Cannabidiol in patients with treatment-resistant epilepsy: an open-label interventional trial. *Lancet Neurol* 15:270–278.

Devinsky O, Patel AD, Cross JH, Villanueva V, Wirrell EC, Privitera M, Greenwood SM, Roberts C, Checketts D, VanLandingham KE et al.; GWPCARE3 Study Group (2018a) Effect of Cannabidiol on Drop Seizures in the Lennox-Gastaut syndrome. *N Engl J Med* 378:1888–1897.

Devinsky O, Patel AD, Thiele EA, Wong MH, Appleton R, Harden CL, Greenwood S, Morrison G, and Sommerville K; GWPCARE1 Part A Study Group (2018b) Randomized, dose-ranging safety trial of cannabidiol in Dravet syndrome. *Neurology* 90:e1204–e1211.

El-Khateeb E, Achour B, Al-Majdoub ZM, Barber J, and Rostami-Hodjegan A (2021) Non-uniformity of Changes in Drug-Metabolizing Enzymes and Transporters in Liver Cirrhosis: Implications for Drug Dosage Adjustment. *Mol Pharm* 18:3563–3577.

Elmes MW, Kaczocha M, Berger WT, Leung K, Ralph BP, Wang L, Sweeney JM, Miyauchi JT, Tsirka SE, Ojima I et al. (2015) Fatty acid-binding proteins (FABPs) are intracellular carriers for Δ9-tetrahydrocannabinol (THC) and cannabidiol (CBD). *J Biol Chem* 290:8711–8721.

Epidiolex. (2020) Package insert. Greenwich Biosciences, Inc., Carlsbad, CA. https://www.accessdata.fda.gov/drugsatfda_docs/label/2020/210365s005s006s007lbl.pdf. Accessed on Sep 21, 2022.

Epidyolex. (2019) Package insert. GW Pharma (International) B.V., Amersfoort, The Netherlands. https://www.ema.europa.eu/en/documents/product-information/epidyolex-epar-product-information_en.pdf. Accessed on Sep 21, 2022.

Heimbach T, Chen Y, Chen J, Dixit V, Parrott N, Peters SA, Poggesi I, Sharma P, Snoeys J, Shebley M et al. (2021) Physiologically-Based Pharmacokinetic Modeling in Renal and Hepatic Impairment Populations: A Pharmaceutical Industry Perspective. *Clin Pharmacol Ther* 110:297–310.

Jiang R, Yamaori S, Takeda S, Yamamoto I, and Watanabe K (2011) Identification of cytochrome P450 enzymes responsible for metabolism of cannabidiol by human liver microsomes. *Life Sci* 89:165–170.

Johnson TN, Bonner JJ, Tucker GT, Turner DB, and Jamei M (2018) Development and applications of a physiologically-based model of paediatric oral drug absorption. *Eur J Pharm Sci* 115:57–67.

Johnson TN, Small BG, Berglund EG, and Rowland Yeo K (2021) A best practice framework for applying physiologically-based pharmacokinetic modeling to pediatric drug development. *CPT Pharmacometrics Syst Pharmacol* 10:967–972.

Khojasteh SC, Prabhu S, Kenny JR, Halladay JS, and Lu AYH (2011) Chemical inhibitors of cytochrome P450 isoforms in human liver microsomes: a re-evaluation of P450 isoform selectivity. *Eur J Drug Metab Pharmacokinet* 36:1–16.

Koch N, Jennotte O, Gasparrini Y, Vandenbroucke F, Lechanteur A, and Evrard B (2020) Cannabidiol aqueous solubility enhancement: Comparison of three amorphous formulations strategies using different type of polymers. *Int J Pharm* 589:119812.

Ladumor MK, Bhatt DK, Gaedigk A, Sharma S, Thakur A, Pearce RE, Leeder JS, Bolger MB, Singh S, and Prasad B (2019a) Ontogeny of Hepatic Sulfotransferases and Prediction of Age-Dependent Fractional Contribution of Sulfation in Acetaminophen Metabolism. *Drug Metab Dispos* 47:818–831.

Ladumor MK, Thakur A, Sharma S, Rachapally A, Mishra S, Bobe P, Rao VK, Pammi P, Kangne H, Levi D et al. (2019b) A repository of protein abundance data of drug metabolizing enzymes and transporters for applications in physiologically based pharmacokinetic (PBPK) modelling and simulation. *Sci Rep* 9:9709.

Lapham K, Bauman J, Walsky R, Bourcier K, Giddens G, Obach R, Hyland R, and Goosen T (2012) Digoxin and tranilast identified as novel isoform-selective inhibitors of human UDP-glucuronosyltransferase 1A9 (UGT1A9) activity. *Drug Metab Rev* 44:82.

Lapham K, Callegari E, Cianfrogna J, Lin J, Niosi M, Orozco CC, Sharma R, and Goosen TC (2020) In vitro characterization of ertugliflozin metabolism by UDP-glucuronosyltransferase and cytochrome P450 enzymes. *Drug Metab Dispos* 48:1350–1363.

Mazur A, Lichti CF, Prather PL, Zielinska AK, Bratton SM, Gallus-Zawada A, Finel M, Miller GP, Radomińska-Pandya A, and Moran JH (2009) Characterization of human hepatic and extra-hepatic UDP-glucuronosyltransferase enzymes involved in the metabolism of classic cannabinoids. *Drug Metab Dispos* 37:1496–1504.

Meseguer ES, Elizalde MU, Borobia AM, and Ramírez E (2021) Valproic Acid-Induced Liver Injury: A Case-Control Study from a Prospective Pharmacovigilance Program in a Tertiary Hospital. *J Clin Med* 10:1153.

Ohlsson A, Lindgren JE, Andersson S, Agurell S, Gillespie H, and Hollister LE (1986) Single-dose kinetics of deuterium-labelled cannabidiol in man after smoking and intravenous administration. *Biomed Environ Mass Spectrom* 13:77–83.

Perkins D, Butler J, Ong K, Nguyen T-H, Cox S, Francis B, Mcintosh M, and Lilley B (2020) A Phase 1, Randomised, Placebo-Controlled, Dose Escalation Study to Investigate the Safety, Tolerability and Pharmacokinetics of Cannabidiol in Fed Healthy Volunteers. *Eur J Drug Metab Pharmacokinet* 45:575–586.

Poulin P and Theil F-P (2002) Prediction of pharmacokinetics prior to in vivo studies. 1. Mechanism-based prediction of volume of distribution. *J Pharm Sci* 91:129–156.

Prasad B, Bhatt DK, Johnson K, Chapa R, Chu X, Salphati L, Xiao G, Lee C, Hop CECA, Mathias A et al. (2018) Abundance of Phase 1 and 2 Drug-Metabolizing Enzymes in Alcoholic and Hepatitis C Cirrhotic Livers: A Quantitative Targeted Proteomics Study. *Drug Metab Dispos* 46:943–952.

Qian Y and Markowitz JS (2022) Prediction of Carboxylesterase 1-Mediated In Vivo Drug Interaction between Methylphenidate and Cannabinoids using Static and Physiologically Based Pharmacokinetic Models. *Drug Metab Dispos* 50:968–979.

Roberts MS and Rowland M (1986) Correlation between in-vitro microsomal enzyme activity and whole organ hepatic elimination kinetics: analysis with a dispersion model. *J Pharm Pharmacol* 38:177–181.

Rose RH, Turner DB, Neuhoff S, and Jamei M (2017) Incorporation of the Time-Varying Postprandial Increase in Splanchnic Blood F into a PBPK Model to Predict the Effect of Food on the Pharmacokinetics of Orally Administered High-Extraction Drugs. *AAPS J* 19:1205–1217.

Samara E, Bialer M, and Mechoulam R (1988) Pharmacokinetics of cannabidiol in dogs. *Drug Metab Dispos* 16:469–472.

Sharma S, Suresh Ahire D, and Prasad B (2020) Utility of Quantitative Proteomics for Enhancing the Predictive Ability of Physiologically Based Pharmacokinetic Models Across Disease States. *J Clin Pharmacol* 60 (Suppl 1):S17–S35.

Taylor L, Crockett J, Tayo B, and Morrison G (2019) A Phase 1, Open-Label, Parallel-Group, Single-Dose Trial of the Pharmacokinetics and Safety of Cannabidiol (CBD) in Subjects With Mild to Severe Hepatic Impairment. *J Clin Pharmacol* 59:1110–1119.

Taylor L, Gidal B, Blakey G, Tayo B, and Morrison G (2018) A Phase I, Randomized, Double-Blind, Placebo-Controlled, Single Ascending Dose, Multiple Dose, and Food Effect Trial of the Safety, Tolerability and Pharmacokinetics of Highly Purified Cannabidiol in Healthy Subjects. *CNS Drugs* **32**:1053–1067.

Tayo B, Taylor L, Sahebkar F, and Morrison G (2020) A Phase I, Open-Label, Parallel-Group, Single-Dose Trial of the Pharmacokinetics, Safety, and Tolerability of Cannabidiol in Subjects with Mild to Severe Renal Impairment. *Clin Pharmacokinet* **59**:747–755.

Tsamandouras N, Rostami-Hodjegan A, and Aarons L (2015) Combining the 'bottom up' and 'top down' approaches in pharmacokinetic modelling: fitting PBPK models to observed clinical data. *Br J Clin Pharmacol* **79**:48–55.

Verbeeck RK (2008) Pharmacokinetics and dosage adjustment in patients with hepatic dysfunction. *Eur J Clin Pharmacol* **64**:1147–1161.

Watkins PB, Church RJ, Li J, and Knappertz V (2021) Cannabidiol and Abnormal Liver Chemistries in Healthy Adults: Results of a Phase I Clinical Trial. *Clin Pharmacol Ther* **109**:1224–1231.

Yamamoto T, Itoga H, Kohno Y, Nagata K, and Yamazoe Y (2005) Prediction of oral clearance from in vitro metabolic data using recombinant CYPs: comparison among well-stirred, parallel-tube, distributed and dispersion models. *Xenobiotica* **35**:627–646.

Address correspondence to: Jashvant D. Unadkat, Department of Pharmaceutics, University of Washington, Box 357610, Seattle, WA 98195. E-mail: jash@uw.edu